A small inorganic-organic material based on anthraquinone-decorated cyclophosphazene as cathode for aqueous electrolyte zinc-ion batteries

Nazmiye Kılıç, Serkan Yeşilot, Selin Sariyer, Arpita Ghosh, Adem Kılıç, Ozlem Sel, Rezan Demir-Cakan

A Small Inorganic-Organic Material Based on Anthraquinone Decorated Cyclophosphazene as Cathode for Aqueous Electrolyte Zinc-Ion Batteries

Nazmiye Kılıç[a], Serkan Yeşilot[a], Selin Sariyer[b,c], Arpita Ghosh[d,e], Adem Kılıç[a], Ozlem Sel[d,e*] and Rezan Demir-Cakan[b,c*]*

[a] Department of Chemistry, Gebze Technical University, Gebze, Kocaeli, 41400, Turkey

[b] Institute of Nanotechnology, Gebze Technical University, Gebze, Kocaeli, 41400, Turkey

[c] Department of Chemical Engineering, Gebze Technical University, Gebze, Kocaeli, 41400, Turkey

[d] Chimie du Solide et de l'Energie, UMR 8260, Collège de France, 11 Place Marcelin Berthelot, 75231 Paris Cedex 05, France

[e] Réseau sur le Stockage Electrochimique de l'Energie (RS2E), CNRS FR 3459, 33 Rue Saint Leu, 80039 Amiens Cedex, France

Keywords: Aqueous electrolyte, Zn-ion battery, Anthraquinone, Cyclophosphazene, Small Inorganic-Organic Material.

Abstract

The small inorganic-organic material (hexakis(2-anthraquinonyloxy) cyclotriphosphazene - **THAQ**) is synthesized from the commercially available starting materials in a one-step reaction and its relevance as an aqueous zinc-ion battery cathode material is assessed. The **THAQ** structure is verified by using appropriate standard spectroscopic methods such as ^{31}P and ^{1}H Nuclear magnetic resonance spectroscopy and MALDI-TOF (Matrix-assisted laser desorption/ionization-time-of-flight). The charge storage mechanism and the evolution of the interfacial properties of the **THAQ** are investigated through several *ex-situ* analysis (Fourier-transform infrared spectroscopy and X-ray photoelectron spectroscopy) and electrochemical quartz crystal microbalance, indicating both Zn^{2+} and H^{+} participation. The insoluble **THAQ** electrode demonstrates a remarkable electrochemical performance with over 150 mAh/g at 30 C, as well as an ultra-long term cycling (>30000 cycles) stability at ultra-high current rate (100 C). The outstanding electrochemical performance turns out to be governed by the multiple nucleophilic carbonyl active sites and increased π-π interaction of **THAQ**, and its lower band gap compared to the anthraquinone counterparts, verified by density functional theory calculations. Overall, this work is the first report revealing the nature of charge carries of inorganic-organic material system, specifically anthraquinone decorated cyclophosphazene, obtained by a facile and cost-effective methods that further demonstrates excellent electrochemical performance.

1. Introduction

The development of efficient energy storage systems, more specifically rechargeable batteries, is of great importance for the worldwide energy problem. Among the novel rechargeable batteries, lithium-ion batteries are widely investigated because of their high energy and power densities. However, drawbacks such as safety problems (*i.e.,* hazardous lithium dendrites and the use of organic-based electrolytes) and cost issues due to the limited lithium supply seriously restrict their large-scale applications.[1] These limitations have directed the research fraternity to focus on higher safety and sustainable battery options in recent years. In this respect, aqueous ion batteries (AIBs) are thought to be a promising class of batteries for energy storage systems because of their lower price, higher operational safety, higher ionic conductivity, environmental benignity, and water stability.[2]

In particular, aqueous electrolyte Zn-ion batteries (ZIBs) have been the focus over the past years because of the low standard redox potential (0.76 V vs. standard hydrogen electrode (SHE)) and high theoretical capacity (820 mAh g^{-1}) of the Zn anode that operates at mild acidic electrolytes. For building high-performance ZIBs, manganese-based materials, vanadium-based materials, or Prussian blue analogs are the most widely investigated inorganic compounds that have been simply coupled with Zn metal anode.[3] Nevertheless, there are many roadblocks for practical applications, such as phase changes and insufficient stability of the inorganic cathodes upon cycling.[4] Seeking for organic alternatives, quinones are carbonyl-based compounds and are ubiquitous in nature, which constitute a promising class of sustainable and environment-friendly electrode materials.[5-7]

Quinone compounds indeed have been widely presented as cathode active materials for organic batteries because of their high theoretical specific capacities and flexible molecule pattern.

Moreover, the working potential of the quinone-based electrodes can be tailored by altering the functional groups.[8-10] However, as of many other organic based cathodes, quinone electrodes in organic electrolytes suffer from fast capacity fading and short cycle life due to their dissolution, while in aqueous medium, they have been proven to be stable with an excellent redox activity.[11-13] Generally, ZIBs based on carbonyl compounds operate *via* reversible coordination of Zn^{2+} ion with the carbonyl groups during the electrochemical process, encouraging electrochemical reversibility.[14] In the light of acquired knowledge on organic-based electrode materials, numerous cathodes have been designed or modified for rechargeable ZIBs, presenting electrochemical behaviors which are suitable for coupling with zinc metal anodes.[5] Small quinone compounds were also investigated as cathodes for aqueous ZIBs (*i.e.*, 1,4-naphthoquinone (1,4-NQ),[15] 9,10-phenanthrenequinone (9,10-PQ),[16] calix[4]quinone (C4Q),[17] 1,2-naphthoquinone (1,2-NQ),[17] 9,10-anthraquinone (9,10-AQ),[17] or pyrene 4,5,9,10 tetraone (PTO),[18]). For example, Zhao *et al.* fabricated a calix[4]quinone (C4Q) molecule, where each benzoquinone unit is linked by a C-C single bond to form a bowl-like structure, exhibited a high specific capacity of 335 mAh g^{-1}.[17] Guo *et al.* reported PTO cathode with four active carbonyl groups with a high capacity of 336 mAh g^{-1} at 0.04 A g^{-1} [19]. A type of quinone compound, triangular phenanthrenequinone (PQ-Δ) structure, allowed the co-insertion of Zn^{2+} and water delivering a 225 mAh g^{-1} at 30 mA g^{-1}.[20] Beside these studies, many other types of quinone-based materials have been explored as cathodes.[21-25] One of the most important reasons for the preference of small cathode molecule is easy synthesis and lower cost. To avoid the dissolution problem encountered in battery systems, small molecules were modified by relatively more complex and multiple synthesis steps.[12] Therefore, there is still room for the development of new materials synthesized with a facile synthesis route providing both insolubility in electrolytes

and high capacity in order to preserve the advantages of small cathode molecule to be used in battery systems. Thus, the aim of the study is to produce a small inorganic-organic material with the desired properties by an effortless and low cost synthesis method.

The phosphorous-nitrogen compounds known as phosphazenes attract attention due to their synthetic flexibility and organic-inorganic structures.[26] The phosphazenes are used in a wide variety of applications due to their characteristic properties such as thermal stability, electrical conductivity, liquid crystallinity, and biomedical activity.[27, 28] Especially, the electrochemical/thermal stability of these compounds leads to their potential to be used for many energy storage systems as cathode[29, 30], anode materials[31], or separators.[32] The hexachlorocyclotriphosphazene (HCCP) structure is one of the most well-known cyclic structures in the phosphazene chemistry formed by bonding of P and N atoms in a planar structure with D_{3h} symmetry. HCCP derivatives can be prepared through substitution reactions of the chlorides with side groups.[33] The phosphorus atom can be easily organized to bear a wide range of different substituents and can redesign the material characteristics with respect to their applications.[26, 28] HCCP derivatives are also known to have high thermal stability and are extremely sensitive to nucleophilic reactions under basic conditions, so it was chosen, in the present work, as a core to provide the desired properties in efficient cathode materials.

Herein, a small inorganic-organic material based on anthraquinone decorated cyclophosphazene (**THAQ**) is synthesized and applied as a cathode material for aqueous ZIBs. **THAQ** offers potential cathode material properties with high thermal stability and insolubility in aqueous electrolytes, as well as multiple electroactive sites for ZIBs, which resulted in propitious electrochemical performance. Prior to the electrochemical studies, **THAQ** was characterized by using appropriate standard spectroscopic methods, including ^{31}P and ^{1}H NMR (Nuclear Magnetic

Resonance) spectroscopy, MALDI-TOF, FT-IR (Fourier-transform infrared spectroscopy), TGA (Thermogravimetric analysis) and simple flame test. Thermal stability, flammability, and ignitability of **THAQ** and 2-hydoxyanthraquione (HAQ) were investigated by TGA and burning tests. The electrochemical performance as an aqueous ZIB cathode material was evaluated in 2 M $ZnSO_4$ aqueous electrolyte. *In-situ* EQCM (electrochemical quartz crystal microbalance) with motional resistance monitoring (EQCM-R) has been used to probe the possible role of multi-species (Zn^{2+} and H^+) in the charge compensation mechanism and the evolution of electrode/electrolyte interface during electrochemical cycling.[34-36] The dissolution tests were carried out by UV-Vis spectroscopy in an aqueous solution for **THAQ** and AQ. Compositional and structural information are investigated by *ex-situ* X-ray diffraction (XRD), scanning electron microscopy (SEM), and energy-dispersive X-ray spectroscopy analyses (EDS). The Zn^{2+}/H^+ ion coordination mechanism of **THAQ** was further examined by using *ex-situ* FT-IR, X-ray photoelectron spectroscopy (XPS) analyses and density functional theory (DFT) calculations.

Experimental

Material

2-hydroxyanthraquinone (HAQ), anthraquinone (AQ), sodium hydride (60% suspension in mineral oil-NaH), hexane and tetrahydrofuran (THF) were purchased from Sigma-Aldrich. Hexachlorocyclotriphosphazene (HCCP) was also obtained from Sigma-Aldrich (98%) and further purified by vacuum sublimation before reaction. The deuterated solvent (DMSO(Dimethyl sulfoxide)-d_6) for NMR spectroscopy was obtained from Merck. Analytical thin layer chromatography (TLC) was performed on Silica gel plates (Merck, Kieselgel 60, 0.25 mm

thickness) with F254 indicator. All other chemicals and solvents were reagent grade quality and were obtained from commercial suppliers.

2.2. Synthesis of hexakis(2-anthraquinonyloxy)cyclotriphosphazene (THAQ)

HAQ (1.0 g, 4.46 mmol) and dry sodium hydride (NaH) (0.2 g, 4.46 mmol) were dissolved in dry THF (10 mL) in argon atmosphere at room temperature. The HCCP containing solution (0.24 g, 0.68 mmol in 4 mL THF) was taken into dropping funnel and added drop by drop to reaction mixture. The reaction mixture was stirred at the boiling point of solvent (~70-80 °C) for 96 h and in between controlled by thin layer chromatography (TLC). The reaction mixture filtered off and volatile materials were evaporated under vacuum. The resulting product was subjected to column chromatography on silica gel using hexane: ethyl acetate (1:1) as the mobile phase. The last eluate was designated as **THAQ** compound and was subjected to further analyses (0.214 g, yield 57%).

2.3. Material Characterization

^{31}P NMR and ^{1}H NMR spectra were conducted by NMR on a Varian INOVA 500-MHz spectrometer in DMSO-D_6 (85% H_3PO_4 and TMS (Tetramethylsilane) as reference). Mass analysis was recorded by a Bruker MALDI-TOF (matrix-assisted laser desorption/ionization-time-of-flight) spectrometer using 1,8,9-Anthracenetriol (Dithranol-DIT) as a matrix for **THAQ**. FT-IR spectra were recorded on a Bruker Alpha-P in ATR in the range of 650-4000 cm^{-1}. Functional groups of HAQ and **THAQ** were determined by FT-IR method. To qualitatively determine the presence of halogen, simple flame tests were carried out with a clean copper wire on a Bunsen burner. The thermal property of the **THAQ** and HAQ were investigated on Mettler Toledo TGA/SDTA 851 thermogravimetric analyser (TGA) at a heating rate of 10 C min^{-1} under argon flow (50 mL min^{-1}) between 25 and 700 °C. The surface morphology and elemental analysis of the **THAQ/KB** was investigated by scanning electron microscopy (SEM) (FEI PHILIPS, XL30

SFEG SEM) coupled with energy-dispersive X-ray spectroscopy (EDS). XRD patterns of **THAQ/KB** electrode (pristine and full discharged), $ZnSO_4.7H_2O$, and $(Zn_4(OH)_6SO_4 \cdot 0.5H_2O$ were recorded by using a Bruker-D8 Advance diffractometer (Bruker AXS).

The burning tests of **THAQ** and HAQ were carried out on a Bunsen burner using ~2 mg of the sample with a spatula. The specific ignition time (SIT) and the self-extinguish time (SET) were determined by the burning test. Limiting oxygen index (LOI) value was calculated from TGA data using Van Krevelen and Hoftyzer's equation.[37]

$$LOI=17.5 + 0.4*\text{Char yield(CR)}$$

Dissolution tests were also performed to evaluate the solubility of **THAQ** and AQ in the aqueous medium, for the pristine and discharged samples. All dissolution tests were recorded with a Shimadzu 2101 UV spectrophotometer with quartz cuvettes at room temperature. XPS spectra were recorded using a Specs Flex-Mod system with a monochromatic Al Kα X-ray source. Elementary mapping was performed to reveal the chemical distribution of atoms on the surface of the **THAQ** electrode after the electrochemical cycling process.

2.4. Electrochemical Measurements

THAQ/KB electrode was prepared by mixing the Ketjen black (KB) and **THAQ** powder at a weight ratio of 70:30 (KB:**THAQ**) in a mortar for half an hour. The weight of active materials was set to 1.5-2 mg. Zinc metal anode, 2 M $ZnSO_4$ aqueous electrolyte and **THAQ/KB** cathode were used in the Swagelok type cell configuration. All electrochemical performance tests were carried out employing Bio-Logic VMP-3 electrochemical workstation in a voltage range of 0.1-1.7 V (*vs.* Zn^{2+}/Zn). Electrochemical impedance spectroscopy (EIS) was conducted at OCV in the frequency range from 1 MHz to 10 mHz with a potential perturbation amplitude of 5 mV, in two-electrode Swagelok cells where zinc metal was used as both working and reference electrodes.

EQCM-R experiment were carried out using AT-cut gold-patterned 9 MHz quartz resonators (AWS, Valencia, Spain) as substrates. A homogeneous slurry containing the active material (**THAQ**) was prepared and drop-casted on the gold electrode (0.2 cm^2) of the quartz resonator. For the slurry preparation, the **THAQ** has been mixed thoroughly with Ketjen Black (KB) and PVdF(Polyvinylidene fluoride) in 24:56:20 (**THAQ**:KB:PVdF) ratio prior to be dispersing in NMP, in order to ensure the binding and the electrical conductivity of the resulting composite electrode. After drop-casting, the QCM resonators were dried in a hot-plate at 80 °C. The active mass loading (**THAQ**) has been kept as low as possible (~ 7.14 μg), to have a thin layer covering the gold electrode of the quartz resonator. As prepared electrodes were then subjected to electrochemical measurements performed with Bio-Logic electrochemical workstation (Bio-Logic SP200) coupled with a SEIKO QCM922A device, which permitted the frequency (Δf) and the motional resistance changes (ΔR_m) to be simultaneously monitored. As prepared QCMs, platinum wire and Ag/AgCl electrode were used as the working, counter, and reference electrodes, respectively. All the EQCM tests have been performed in 2 M $ZnSO_4$ aqueous electrolyte.

2.5 DFT Calculation

Theoretical calculations were performed to investigate the charge compensation mechanism of the **THAQ**. DFT calculations were performed by the Gaussian 16W software[38] package to gain structural information of the molecules. On the basis of the optimized structure of **THAQ** molecule (B3LYP/6-31G(d,p)[17] and wB97XD/6-31G (d,p)[39]), the molecular electrostatic potential (MESP) method was applied to predict the electrostatic potential map of **THAQ**. The MESP analysis was also done to deduce the possible Zn/H uptake positions using the Gaussian 16W software package. The single point energy (SPE) and frequency calculations of involving Zn species were calculated by B3LYP basis set LANL2DZP level.[40]The final Gibbs free energy is

the sum of electronic energy and thermal correction from the frequency analysis. Also, partial optimization (freeze atoms) was performed with a T* structure because of the chemical structure and interactions of **THAQ**. The binding energy (*E*b) was obtained by calculating the Gibbs free energy difference between the total energy of the complex ($G_{T*HxZny}$) and the sum of individual energy of the ions (G_{H^+} , $G_{Zn^{2+}}$) and (G_{T*}), respectively[25], which was expressed as follows:

$$E\,b\; =\; \Delta G\; =\; (G_{T*HxZny}) - (G_{T*}) - \; xG_{H+}\; -\; yG_{Zn2+}$$

3. Results and discussion

THAQ was synthesized by one-step reaction of hexachlorocyclotriphosphazene and 2-hydroxyanthraquinone, in the presence of NaH in THF (Figure 1a). The ^{31}P NMR spectrum of **THAQ** exhibited a single peak at 7.15 ppm, indication of substitution of all chlorine atoms of HCCP (Figure 1b). The complete substitution was further supported by the disappearance of the HCCP peak, which is supposed to be at approximately 19 ppm, as well as the absence of specific chlorine color in the simple flame test (inset Figure 1a). The simple flame test is used to qualitatively examine the presence of certain elements[41, 42], especially metals and halogens in chemical compounds. Specific green color of chlorine in HCCP was no longer observed for that of **THAQ**. In the ^{1}H NMR spectrum, the peaks located at 8.08 and 6.60 ppm suggested the five types of aromatic H atoms (also integration ratios 1:1:1:2:2) in **THAQ** (Figure 1b). In addition, the exact m/z value of 1475.05 was found by MALDI TOF, which is in-agreement with the calculated theoretical value of 1474.18, ascertaining the successful synthesis of the **THAQ** (Figure 1c). The FT-IR spectra of **THAQ** and HAQ are shown in Figure 1d. The characteristic vibrations of C=O and C=C peaks are located at 1677 cm^{-1} and 1588 cm^{-1}, respectively, which correspond to anthraquinone side groups.[43] The characteristic vibrations peaks of HCCP at 1176 and 1152 cm^{-1} clearly belongs to P=N and P-N vibrations.[44] Compared with the FT-IR spectrum of HAQ, the

vibrations of the hydroxyl group (-OH) (3339 cm^{-1}) disappeared in the FT-IR spectrum of **THAQ**, instead new peaks appear that are assigned to the P=N (1176 cm^{-1}), P-N (1132 cm^{-1}) and P-O-C (923 cm^{-1}).

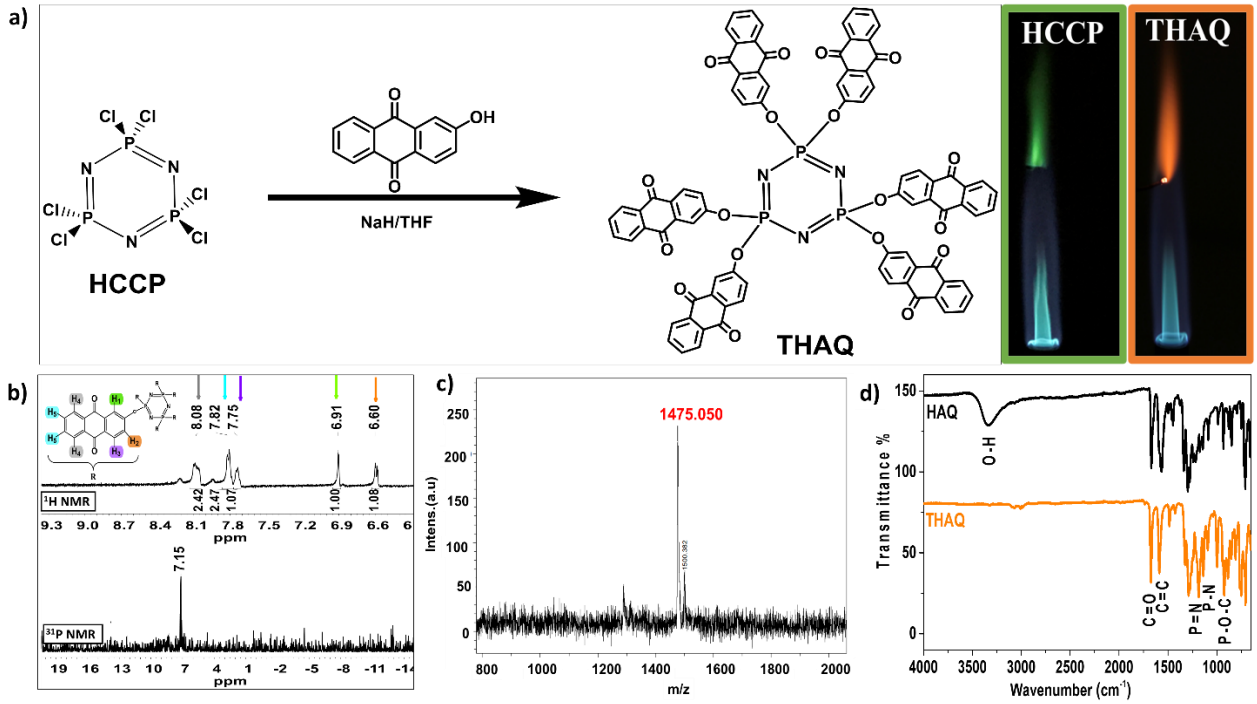

Figure 1. a) Synthetic route of **THAQ (**inset simple flame test results of HCCP and **THAQ**). The characterization of **THAQ** in b) ^{31}P and ^{1}H NMR spectra of **THAQ** (in d_6-DMSO), c) MALDI-TOF spectrum for **THAQ** and d) FT-IR spectra of HAQ and **THAQ**.

The thermal stability of **THAQ** and HAQ were compared with TGA performed between 25-700 °C (Figure 2a). The first obvious weight loss of **THAQ** is observed at approximately 120 °C and 59.2 wt.% remained up to 700 °C, versus only 2.2 % for HAQ. The specific ignition time (SIT), specific self-extinguish time (SET), and the limiting oxygen index (LOI) values, which determine the flammability and ignitability of materials, were determined by burning test (Figure 2b) and TGA.[37] The calculated LOI of the **THAQ** and HAQ are ~41 and ~18, respectively, determined by the residue char yield from the TGA data. **THAQ** can be classified as self-extinguishing

materials (LOI: 28-100).[45] The SIT and SET values of **THAQ** and HAQ were measured to be 5.23 - 5.11 and 3.99 - 9.17 s, as shown in Figure 2d. In addition, vibrations of P=N and P-O-C bonds are observed in the FT-IR spectrum of **THAQ** after the burning test (Figure 2c).[46] meaning that **THAQ** molecule was preserved its chemical structure to a certain extent upon burning. As a result, the thermal stability of **THAQ** is acceptable and reliable for battery applications.

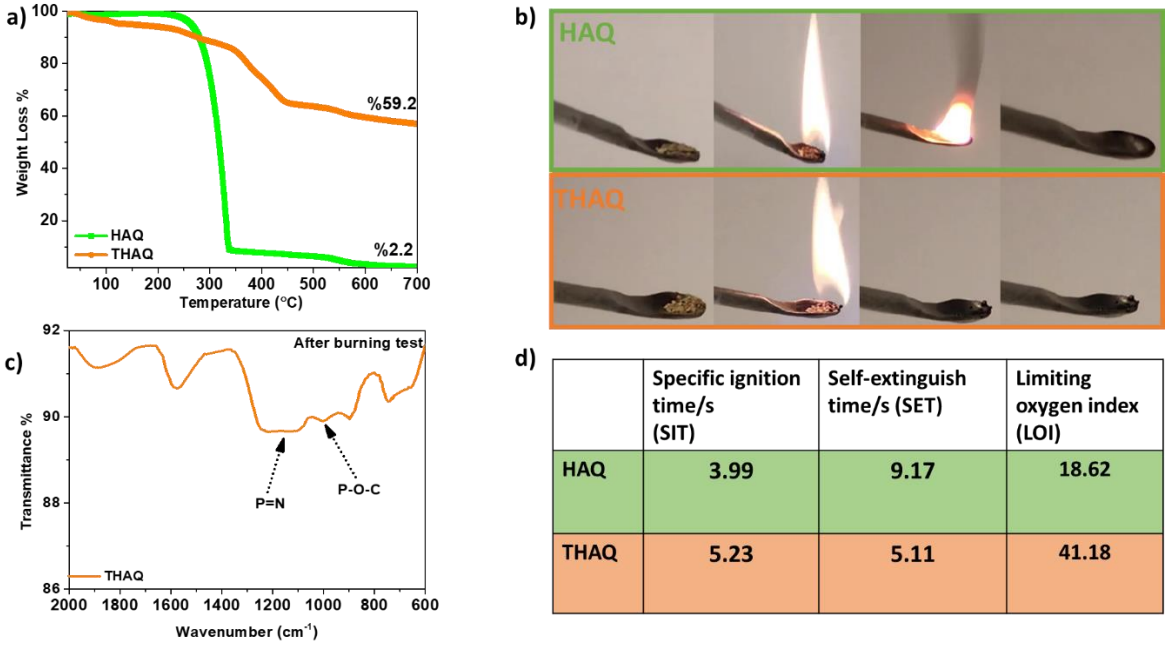

	Specific ignition time/s (SIT)	Self-extinguish time/s (SET)	Limiting oxygen index (LOI)
HAQ	3.99	9.17	18.62
THAQ	5.23	5.11	41.18

Figure 2. a) TGA of HAQ and **THAQ**, b) burning test of HAQ and **THAQ**, c) FT-IR spectrum of **THAQ** after burning test, d) SIT, SET and LOI values of HAQ and **THAQ**.

Redox behavior of the **THAQ/KB** (weight ratio of 30:70) cathode was evaluated by using cyclic voltammetry (CV) between a voltage range of 0.1 and 1.7 V *vs.* Zn^{2+}/Zn (Figure 3a). A pair of redox peaks at scan rate of 1 mV s^{-1} were observed at 0.42 and 0.65 V (*vs* Zn^{2+}/Zn) for the reduction and oxidation, respectively, which was ascribed to the reversible (de)coordination reaction between the charge carrier species and carbonyl group (C=O) of quinone based active

materials.[17] After the initial CV cycle, overlapping consecutive CV curves indicate the high stability of **THAQ/KB** electrode. Moreover, in order to compare the redox behavior of **THAQ/KB**, commercially available anthraquinone (AQ) was used with the same carbon amount (quoted as AQ/KB) electrode. Similarly, AQ/KB electrode demonstrated one reduction and one oxidation peak at 0.38 and 0.73 V *vs.* Zn/Zn^{2+}.[9] The redox peak separation of AQ is more significant in comparison with the **THAQ** composite (Figure S1) that is ascribed to the lower electronic conductivity of AQ resulting from its wider band gap in agreement with the DFT calculations to be discussed below. Electrochemical performance of **THAQ/KB** electrode was further investigated by galvanostatic discharge/charge measurements. **THAQ/KB** cell exhibited stable discharge voltage profiles at different current densities (Figure 3b). The plateau-like voltage behavior of the composite cathode is favorable for attaining a stable voltage output.[15, 17] C-rate performance of the **THAQ/KB** composite cathode delivered discharge capacity of ca. 157, 150, 158, 160, 163 and 167 mAh g^{-1} at a current density of 120, 60, 30, 20, 10 and 5C, respectively, where, 1 C corresponds to ~36 mA g^{-1}. During the rate capability performance test, this electrode showed high discharge capability as well as high Coulombic Efficiency (CE) (~99%). However, the lower CE obtained at relatively lower current density (~95% at a current density of 5C) could be originated from involvement of the proton during the charge compensations.[47] Furthermore, cycling stability performance results of **THAQ/KB** and AQ/KB electrodes at a current density of 30 C (1.1 A g^{-1}) were comparatively presented in Figure 3d. Although AQ/KB composite electrode provided higher first discharge capacity of 277 mAh g^{-1} than **THAQ/KB** (initial discharge capacity of 174 mAh g^{-1}), the cathode exhibited poorer cycling performance. Remarkably, **THAQ/KB** retained its discharge capacity of 144 mAh g^{-1} with a capacity retention of 82.5% after 1000 cycles. Compared with **THAQ/KB** electrode, the deteriorating cycle performance of AQ/KB composite

could be due to the dissolution of the host material in the aqueous medium.[9, 17] Furthermore, ultra-fast current density applied to the **THAQ/KB** can be seen at Figure 3e, in which over 100 mAh g^{-1} capacity was obtained at 100 C during long-term cycling (>30000). Especially, when organic electrode materials utilized in aqueous electrolyte ZIBs were compared, **THAQ/KB** cathode stands out with its ultra-long-term cycling (30000 cycles) stability and capacity retention (63 %) at high current rates (3600 mA g^{-1}), exhibiting superior electrochemical performance (Table S1).

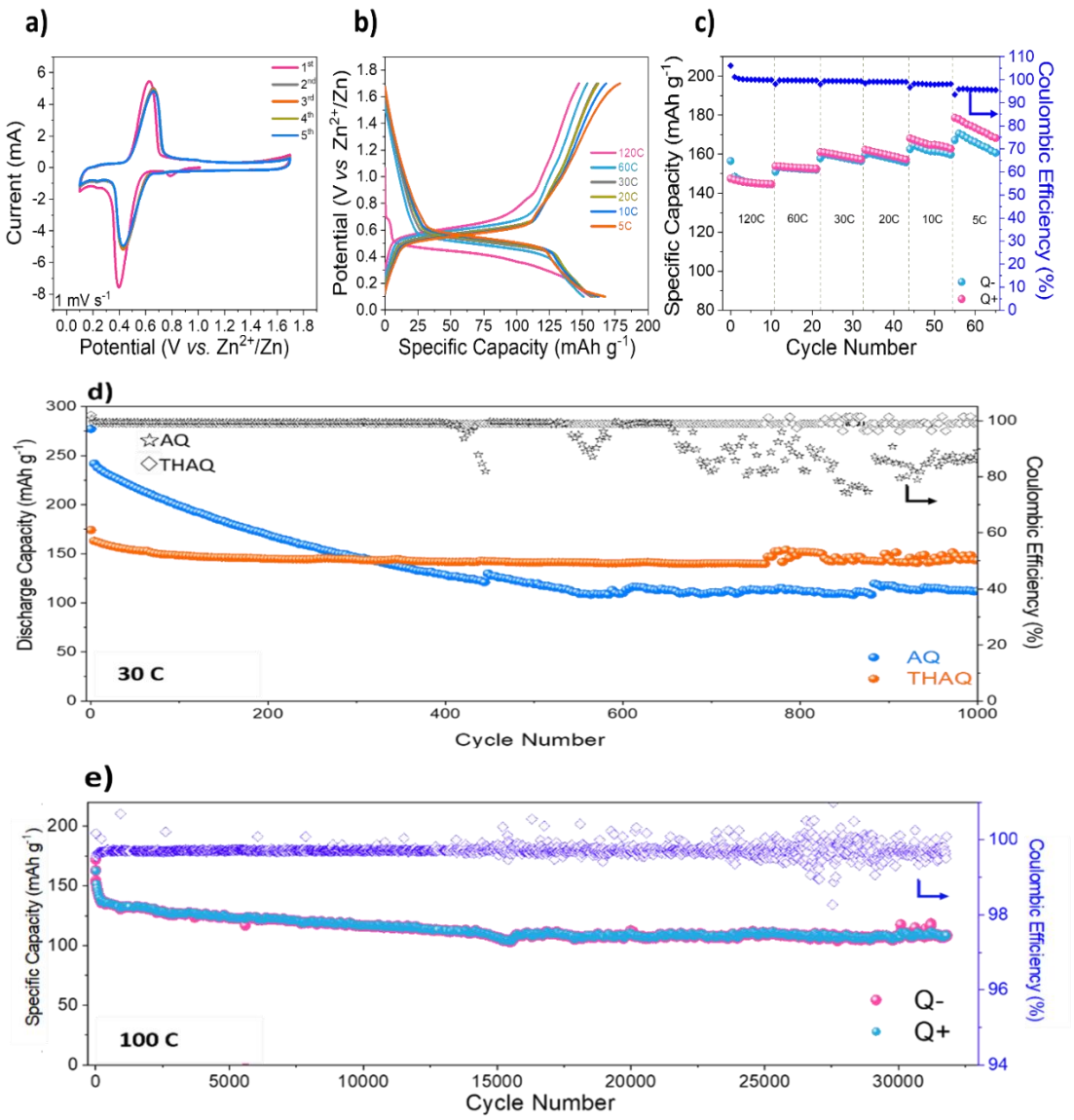

Figure 3. Electrochemical performance of **THAQ/KB** electrode a) CV profiles at a scan rate of 1 $mV.s^{-1}$, b) Discharge/charge profiles at different current densities, c) Discharge/charge capacity at different current densities, d) Comparative cycle performance of **THAQ/KB** with AQ/KB at a current density of 30 C and e) Long-term cycle performance at 100 C of **THAQ/KB**.

Electrochemical impedance spectroscopy (EIS) profile was investigated to reveal the reason for the better rate capability of the synthesized **THAQ** electrode compared with the commercial AQ. In Figure S2c, R1, R2, R3 components of the proposed equivalent circuit refer to electrolyte

resistance (R_e), solid-electrolyte interface resistance (R_{SEI}) and charge-transfer resistance (R_{ct}), respectively.[17] The charge transfer resistances obtained by fitting the EIS data of **THAQ** (Figure S2a) and AQ (Figure S2b) were found to be 38.4 Ω and 903.3 Ω. **THAQ/KB** composite cathode, which resulted in reasonably lower charge transfer resistance, allowing faster ions transportation during discharge/charge processes in accordance with the electrochemical performance.

Dissolution of organic electrode materials especially discharged products is a major drawback, which causes a rapid capacity decay during cycling. Therefore, the solubility of the **THAQ/KB** and AQ/KB electrodes were tested in an aqueous solution. The pristine and discharge states of all solutions were colorless in the water, indicating that **THAQ/KB** and AQ/KB are not dissolved in the aqueous system (inset Figure S3). Further UV-vis spectroscopy tests of **THAQ/KB** and AQ/KB were performed to compare their solubility and it was observed that while **THAQ/KB** did not show any absorption peak, AQ/KB demonstrated an absorption peak at around 270 nm revealing its slight solubility in aqueous medium (Figure S3). Consequently, the insoluble nature of **THAQ** ensured advanced cycling stability in the aqueous battery systems compared to the AQ counterparts.

Numerous studies have been conducted to clarify the charge storage mechanism of organic active materials in aqueous electrolyte zinc-ion batteries. These studies suggest that charge compensation in organic cathodes can be contributed by several mechanisms, including (i) only Zn^{2+} coordination,[19] (ii) individual H^+ intercalation,[40] or (iii) H^+/Zn^{2+} co-insertion.[12, 23, 25, 48, 49]Therefore, herein, the electrochemical reaction mechanism of the **THAQ** electrode was investigated by various *ex-situ* characterization tools at the pristine, discharged, and charged states (Figure 4a). Moreover, theoretical calculations of were performed to investigate the electrochemical properties of the **THAQ** and AQ.

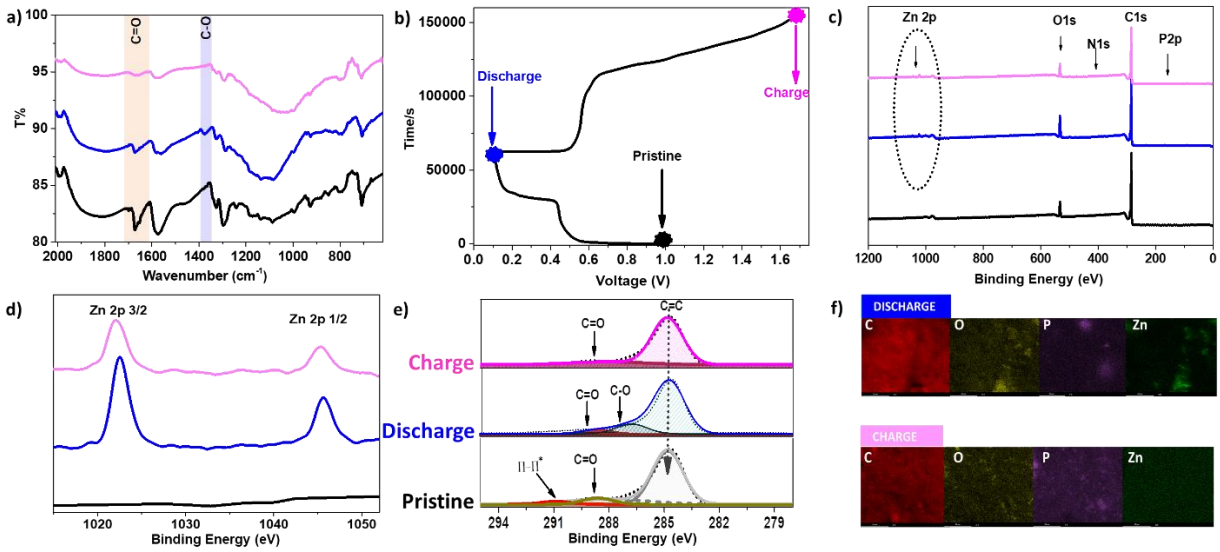

Figure 4. a) Time-dependent evolution of first discharge and charge cycle for **THAQ/KB** electrode cycled at C/5, b) FT-IR spectra of the **THAQ/KB** electrode in the pristine and first charge-discharge states, c) *Ex-situ* XPS spectra of the **THAQ/KB** electrode in the pristine and first charge-discharge states cycled at C/5, d) Zn 2P spectra, and e) C 1S spectra and f) elemental mapping images of C, O, P and Zn components of **THAQ/KB**: carbon (red), oxygen (yellow), phosphorus (purple), and zinc (green).

Firstly, *ex-situ* FT-IR and XPS analyses were performed in which C=O bonds are regarded as active sites to the host charge carrier ions (Figures 4b and 4c). The peak intensity of C=O was monitored by *ex-situ* FT-IR at the pristine, discharged and charged states of **THAQ**. The peak at 1677 cm^{-1} assigned to the stretching vibration of the C=O bonds decreased in intensity and the vibration of C–O bonds at 1379 cm^{-1} appeared upon discharge.[50] During the charging step the reverse change occurred for the C–O. XPS analyses were used to further investigate the mechanism of the charge storage during the cycling process. The survey XPS spectra of

THAQ/KB cathode material confirmed the presence of C, O, P, N for the pristine sample (Figure 4c). Zn-2p XPS spectra of the **THAQ/KB** indicate the appearance of the divalent state Zn element after the first discharge down to 0.1 V, while it becomes much weaker when the electrode is recharged to 1.7 V (Figure 4d). This observation may indicate a slight Zn^{2+} trapping which is in line with the lower initial CE value in Figure 3c. Besides, the C1s XPS spectra of the pristine sample in Figure 4e demonstrates two main peaks attributed to C=O (288.6 eV) ,C=C (284.7 eV) bonds , belonging to the anthraquinone side groups.[51] In addition, the peak, which slight π-π interaction of the THAQ, is located at 291.2 eV. [52] After the first discharge to 0.1 V, the C=O peak has diminished, while that corresponding to C-O, located at 287.2 eV, becomes more prominent, indicating an interaction with the charge carries ions. On the other side, during recharge remaining C=O bond is still observed that is consistent with the FT-IR spectra of the **THAQ/KB**, corresponding to a potential trapping of the charge carrier ions.

Additionally, elemental mappings of the **THAQ/KB** cathode surface display the first discharge-charge process from a macroscopic view (Figure 4f). The spatial distribution of C, O and P elements is similar in both discharge and charge states. However, the intensiveness of Zn mapping decreased from the discharge state to charge, demonstrating participation of Zn^{2+} into charge compensation process. In addition, a typical flake-like morphology of zinc sulfate hydroxide $Zn_4(OH)_6SO_4 \cdot xH_2O$ (x varying between 0.5 and 1) was observed in SEM image of the fully discharged **THAQ/KB** electrode in 2 M $ZnSO_4$ electrolyte (Figure S4). More significantly, EDS (Energy dispersive X-ray spectroscopy) (Figure S4) analysis revealed the elemental composition of the first discharged **THAQ/KB** which possesses the mole ratio of Zn:S about 4, implying the formation of $Zn_4(OH)_6SO_4 \cdot xH_2O$ (ZHS) structure. Furthermore, the new intense peaks at 12.4°, 32.9° and 35.3° are observed in the XRD pattern of the discharged electrode (Figure S5). These

peaks formed after the discharge are indexed as zinc sulfate hydroxide ($Zn_4(OH)_6SO_4 \cdot 0.5H_2O$, JCPDS number 00-044-0674),[23] arising from protons' participation to charge compensation process. As it is well-known, the consumption of protons induces local pH increase, then OH^- reacts with $ZnSO_4$ and H_2O to form the so-called ZHS as a by-product.[53] The results of these *ex-situ* FT-IR, XPS and XRD analyses strengthen the idea that the coordination of both Zn^{2+} cations and as well as H^+ occurs during discharge of the **THAQ/KB** electrode.

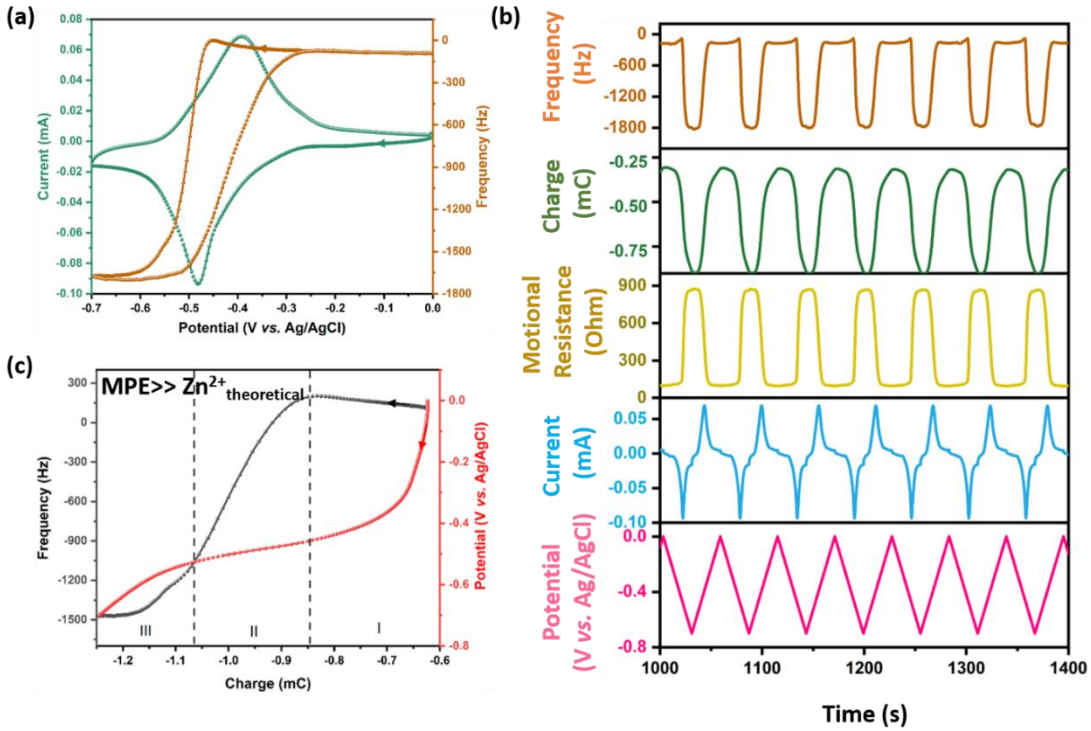

Figure 5. EQCM analyses of **THAQ** composite film deposited on the Au electrode of a 9MHz quartz resonator in 2M $ZnSO_4$ electrolyte. a) CV response and frequency variation curves at 25 mV s^{-1} of the 7th cycle and b) the frequency, charge, motional resistance, current and potential variation as a function of time. The panel c) shows the Δ*frequency vs.* Δ*Charge* and the *potential vs.* Δ*Charge* curve for the reduction scan, corresponding to the EQCM response in panel (a).

In order to further investigate the interfacial charge storage properties of the **THAQ** electrodes, EQCM has been employed as a piezoelectric sensor coupled to electrochemical measurements. We have simultaneously monitored the frequency variation (Δf) during the redox process of the **THAQ** composite thin film. The current and Δf responses of the EQCM measurement carried out at 25 mV s^{-1} are shown in Figure 5a. A pair of pronounced redox peaks can be seen in the CV profiles (Figure 5a) in agreement with the Figure 3a. A significant frequency decrease and increase were observed, during a cathodic and an anodic scan, respectively (Figure 5a). This would imply a major mass increase/decrease during the reduction and oxidation process in Figure 5a. It is noted that these Δf patterns can be correlated to mass variations (Δm), only if the gravimetric conditions are satisfied, then the Sauerbrey equation: $\Delta f = -k_s \times \Delta m$, where k_s is the experimental sensitivity coefficient, can be applied.[34, 54, 55]

During the commence of reduction the Δf changes are small, whereas the prominent decrease can be observed when the potential is approaching -0.48 V. During the reverse scan, again a noticeable frequency increase can be seen in the vicinity of the oxidation peak around -0.42 V. The overall Δf profiles may indicate a charge compensation process by a major cationic response, however the Δf magnitudes are rather high. This observation has prompted us to study the plausible contributions, leading to such high Δf values. Figure 5b depicts the simultaneously measured Δf and motional resistance change (ΔR_m) as a function time, during the EQCM measurements. No significant changes in the profiles (values going back to initial during the reverse scan) ensure the stability of the active material upon cycling. Figure 5c shows an example Δf *vs.* ΔQ profile (at 25 mV s^{-1}), corresponding to the reduction scan of the EQCM response in Figure 5a. This profile can be used to estimate the average mass per electron (MPE) using the following equation: $M.P.E. = n \times F \times \Delta m/\Delta Q$ where, n is the number of the electrons transferred, F is the Faraday's

constant, assuming that the microbalance works as a gravimetric probe. From the MPE analyses, an estimation of the molar mass of the species which participate in the charge compensation during the redox process can be drawn, if there is no other contribution to the frequency changes. The MPE analysis of the middle region shown in Figure 5c lead to a significantly high value, *i.e.,* 859 g mol^{-1}. This high MPE value indicates that another electro-assisted process contributes to the frequency variations, in agreement with our previous work on organic electrodes and also in literature reports.[56, 57] Remarkably high ΔR_m values in Fig. 5b attests this result that the Δf values cannot be attributed to solely a cation coordination process of **THAQ** active material. Overall, the frequency profiles provided by the EQCM demonstrates that the charge compensation process is intertwined with the ZHS formation during the reduction, related to the local pH changes (as a result of coordination of H^+ with the **THAQ**, in agreement with the predictions of the DFT calculations discussed below). In general, such phenomena leads to a viscosity increase at the vicinity of the electrode/electrolyte interface, characterized by the motional resistance (R_m) increase during the EQCM measurements, indicating that the acoustic wave has difficulty to pass through the newly formed interface.[54, 56] The high $\Delta R_m/\Delta f$ ratio in Figure 5b indicates the formation of ZHS at the electrode/electrolyte interface and is fully in line with the *ex-situ* SEM and XRD analyses on the discharged **THAQ/KB** samples (Figure S4 and S5).

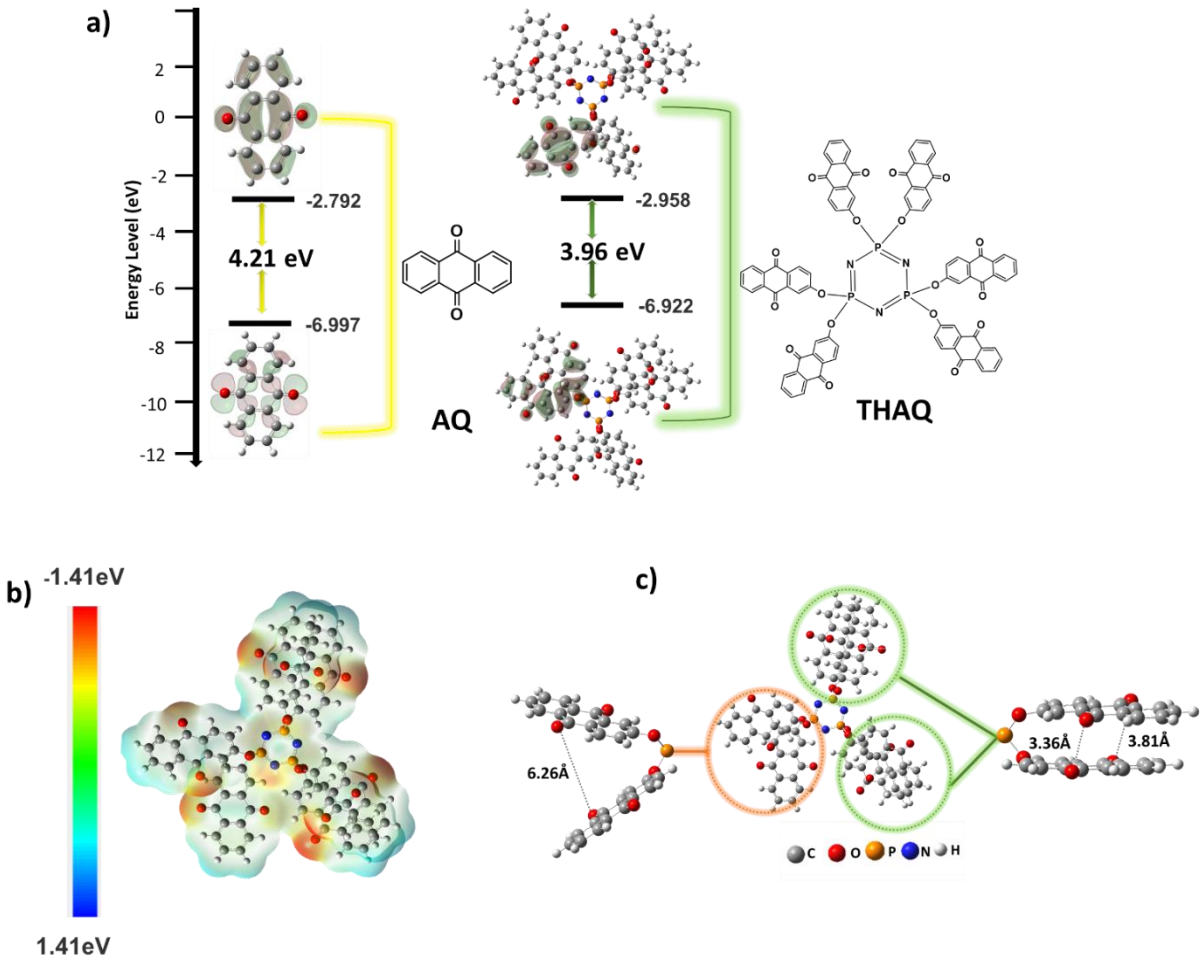

Figure 6. a) HOMO and LUMO plots and band gaps of AQ and **THAQ** b) MESP of **THAQ** molecule c) Side group arrangement of **THAQ** based on optimized geometry.

With the intention of better understanding of the structural arrangement and predicting Zn^{2+}/H^{+} ions coordination mechanism in the **THAQ** molecule, theoretical calculations were carried out using the density functional theory (DFT) with the B3LYP/6-31G(d,p)[17] and B3LYP /LANL2DZP[40] basis set in the gas phase. The optimized geometry of the **THAQ** demonstrated that the distance between anthraquinone units in the **THAQ** structure is less than 4Å (Figure S6a). Hence, the structure was re-optimized using wB97XD/6-31G (d,p) levels which is a more suitable method to determine the non-covalent π-π interactions (Figure S6b-S6c).[39] In addition, the peak

at around 25.65° at the XRD spectrum of THAQ could be attributed to π-π interaction resulting from the polar carbonyl groups in anthraquinone structure (Figure S6d) [58, 59]. The molecular orbitals of AQ and **THAQ** are shown in Figure 6a, including the highest occupied molecular orbital (HOMO) and lowest unoccupied molecular orbital (LUMO) for the comparison of their structural stability. The LUMO energy level of **THAQ** (-2.958 eV) is much lower than that of AQ (-2.792 eV), indicating a higher electron affinity and, thus higher reduction potentials of **THAQ**.[30, 60] Furthermore, due to the increased π-π interaction with the **THAQ** structure, it provides a lower band gap (3.96 eV) compared to the AQ structure (4.20 eV), thus leads to higher electrical conductivity, and as a consequence faster charge transfer, which is beneficial for the improvement of electrochemical properties.[61] Moreover, faster zinc ion transfer coefficient was promoted by also Warburg diffusion process calculation (Figure S7), indicating 3.19×10^{-16} $cm^2\ s^{-1}$ for THAQ/KB and 4.46×10^{-17} $cm^2\ s^{-1}$ for AQ/KB electrode. In addition, the MESP mapping method was used to determine the electroactive regions of the **THAQ** structure with an optimized geometry obtained by considering π-π interactions (Figure 6b. It is well known that this method is performed to investigate the active site for the cation uptake in which more positive sites (toward blue color) are leaning to react with a nucleophilic reagent, whereas the more negative sites (reddish color) prefer to react with an electrophilic reagent.[62] Zn^{2+}/H^+ ions can be assumed as electrophile during the discharge process, that is why the sites with a higher negative region are preferable to other sites for the cation uptake in the discharge reaction.[63] Therefore, the red region indicates strong chemical affinity for cation coordination.[17] Based on the results from MESP mapping, it was demonstrated that electronegative regions of the **THAQ** molecule are mainly located around C=O groups, which are the main active sides for cation coordination (Figure 6b, S8). The structure of **THAQ** has possible sites for multistep cation coordination. The

coordination steps of the **THAQ** structure of zinc ions were constructed based on the MESP method with the single point energy calculations and the side group arrangements (Figure S9). Depending on the Zn coordination, the energy values decreased thermodynamically and the stability of the structures advanced, as expected.[20, 64] Depending on the arrangement of the anthraquinone side groups, there are two different arrangements between the units (Figure 6c). The distance between the anthraquinones is approximately 3-4 Å in the first (green circle), while it is approximately 6Å in the other units (orange circle). Based on this arrangement and the MESP mapping, although the zinc ion is more appropriate for the **THAQ**-Zn coordination, it has not been included because of the large distance (6.26 Å) between Zn and AQ units, as indicated in Figure 6c with orange circle, for the Zn-O bond formation (1.8-2.4Å).[17, 65]

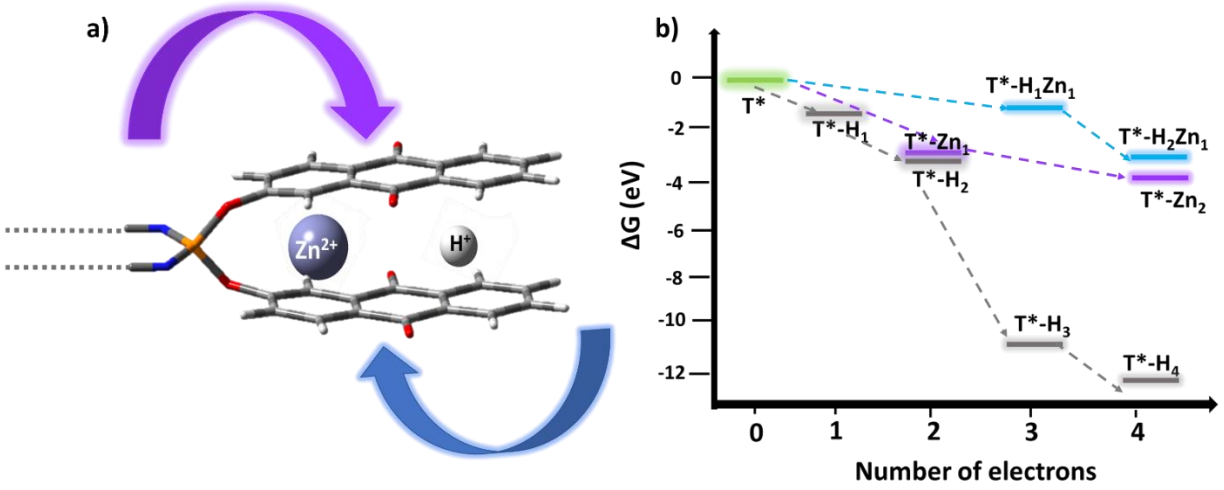

Figure 7. a) The simplified structure of **THAQ** (T*) and b) The calculated ΔG energy for T* ion species.

As it was pointed above in Figure 6c the sides, green highlighted circles are more plausible for Zn coordination. Therefore, one further point of interest is the coordination mechanism of H^+ that was performed with DFT calculations.[40, 48] The coordination mechanism is shown by using the

simplified structure of T* (Figure 7a). In Figure 7b, three main coordination types of ions have been illustrated (H^+, Zn^{2+} or H^+- Zn^{2+}). According to the binding energies, H^+ ion is quite dominant in the coordination steps, especially for the T*-H_1 (-1.43 eV) to T*-H_4 (-12.088 eV) (Table S2). When compared with H^+, the possibility of Zn^{2+} ion is coordination is lower. On the other side, the probability of the formation in steps containing both Zn^{2+} and H^+ ions is also much lower. DFT calculations indicate that the binding of H_4 with T* was shown to be more likely than the other Zn^{2+} containing configurations. However, under experimental conditions Zn ions involvement is more likely to occur where the concentration of Zn^{2+} is much higher than H^+ in 2 M $ZnSO_4$ electrolyte which leads to a competition between Zn^{2+} and H^+.[48] Additionally, the Zn-O (~570 cm^{-1}) and O-H (3450 cm^{-1}) vibrations [25, 63] in the *ex-situ* FT-IR analysis (Figure S10) and the formation of $Zn_4(OH)_6SO_4 \cdot 0.5H_2O$ in the *ex-situ* XRD analysis are observed (Figure S5) demonstrating that experimentally both ions coordination is plausible.

Conclusion

In summary, a facile and straightforward one-step synthesis of a small inorganic-organic material (**THAQ**) from the commercially available starting materials, resulting in a HCCP-bound six anthraquinone structure has been demonstrated. The charge storage mechanism and interfacial processes occurring at the electrode-electrolyte interface were systematically investigated through several *ex-situ* and *in-situ* experimental methods and corroborated with the theoretical calculations (DFT). Multiple redox-active sites and insoluble nature in aqueous electrolyte render **THAQ** electrode a superior cathode material for aqueous ZIBs with ultra-long cycling (>30000 cycles) stability at high current density (3.6 A g^{-1}) in comparison to the commercial anthraquinone counterparts (AQ). This superior performance was associated with the increased π-π

interaction in **THAQ** structure. Theoretical analyses based on DFT reveals the lower band gap of **THAQ** (3.96 eV) compared to the AQ structure (4.20 eV). The reversible ion coordination of **THAQ** was verified by monitoring the carbonyl groups using the time-dependent FT-IR and *ex-situ* XPS. Involvement of proton towards the charge compensation was further identified by the *ex-situ* XRD measurement, which demonstrates the formation of well-known ZHS resulting from the local pH increase. EQCM analyses are well-consistent with XRD analyses, where the reversible ZHS formation/dissolution can be identified indicating both Zn^{2+} and H^{+} participation. Overall, this work is the first report revealing the nature of charge carries of anthraquinone decorated cyclophosphazene obtained by a facile and cost-effective method and demonstrates the development of small cathode molecule based on inorganic-organic material systems to be used in aqueous ZIBs with excellent electrochemical performance.

Declaration of competing interest

The authors declare that they have no known competing financial interests or personal relationships that could have appeared to influence the work reported in this paper.

Acknowledgments

The authors appreciate the financial support from TUBITAK (119N054). TUBITAK ULAKBIM, High Performance and Grid Computing Center (TR-Grid e-Infrastructure) is thanked for the calculations data in the computational chemistry details of this paper.

REFERENCES

[1] G. Fang, J. Zhou, A. Pan, S. Liang, Recent Advances in Aqueous Zinc-Ion Batteries, ACS Energy Letters, 3 (2018) 2480-2501, https://doi.org/10.1021/acsenergylett.8b01426.

[2] L. Wang, J. Zheng, Recent advances in cathode materials of rechargeable aqueous zinc-ion batteries, Materials Today Advances, 7 (2020) 100078, https://doi.org/10.1016/j.mtadv.2020.100078.

[3] N. Zhang, X. Chen, M. Yu, Z. Niu, F. Cheng, J. Chen, Materials chemistry for rechargeable zinc-ion batteries, Chemical Society Reviews, 49 (2020) 4203-4219, http://dx.doi.org/10.1039/C9CS00349E.

[4] C. Luo, L. Xiao, X. Wu, Aqueous zinc ion batteries based on sodium vanadate electrode materials with long lifespan and high energy density, Materials Advances, 3 (2022) 604-610, http://dx.doi.org/10.1039/D1MA00983D.

[5] J. Cui, Z. Guo, J. Yi, X. Liu, K. Wu, P. Liang, Q. Li, Y. Liu, Y. Wang, Y. Xia, J. Zhang, Organic Cathode Materials for Rechargeable Zinc Batteries: Mechanisms, Challenges, and Perspectives, ChemSusChem, 13 (2020) 2160-2185, 10.1002/cssc.201903265.

[6] Y. Li, Y. Lu, Y. Ni, S. Zheng, Z. Yan, K. Zhang, Q. Zhao, J. Chen, Quinone Electrodes for Alkali–Acid Hybrid Batteries, Journal of the American Chemical Society, 144 (2022) 8066-8072, https://doi.org/10.1021/jacs.2c00296.

[7] M. Yu, N. Chandrasekhar, R.K.M. Raghupathy, K.H. Ly, H. Zhang, E. Dmitrieva, C. Liang, X. Lu, T.D. Kühne, H. Mirhosseini, I.M. Weidinger, X. Feng, A High-Rate Two-Dimensional Polyarylimide Covalent Organic Framework Anode for Aqueous Zn-Ion Energy Storage Devices, Journal of the American Chemical Society, 142 (2020) 19570-19578, https://doi.org/10.1021/jacs.0c07992.

[8] D. Kundu, P. Oberholzer, C. Glaros, A. Bouzid, E. Tervoort, A. Pasquarello, M. Niederberger, Organic Cathode for Aqueous Zn-Ion Batteries: Taming a Unique Phase Evolution toward Stable Electrochemical Cycling, Chemistry of Materials, 30 (2018) 3874-3881, https://doi.org/10.1021/acs.chemmater.8b01317.

[9] Q. Wang, X. Xu, G. Yang, Y. Liu, X. Yao, An organic cathode with tailored working potential for aqueous Zn-ion batteries, Chemical Communications, 56 (2020) 11859-11862, http://dx.doi.org/10.1039/D0CC05344A.

[10] Z. Ba, Z. Wang, M. Luo, H.-b. Li, Y. Li, T. Huang, J. Dong, Q. Zhang, X. Zhao, Benzoquinone-Based Polyimide Derivatives as High-Capacity and Stable Organic Cathodes for Lithium-Ion Batteries, ACS Applied Materials & Interfaces, 12 (2020) 807-817, https://doi.org/10.1021/acsami.9b18422.

[11] Y. Liang, Y. Jing, S. Gheytani, K.Y. Lee, P. Liu, A. Facchetti, Y. Yao, Universal quinone electrodes for long cycle life aqueous rechargeable batteries, Nat Mater, 16 (2017) 841-848, https://doi.org/10.1038/nmat4919.

[12] Z. Lin, H.-Y. Shi, L. Lin, X. Yang, W. Wu, X. Sun, A high capacity small molecule quinone cathode for rechargeable aqueous zinc-organic batteries, Nature Communications, 12 (2021) 4424, https://doi.org/10.1038/s41467-021-24701-9.

[13] J. Xie, Q. Zhang, Recent progress in aqueous monovalent-ion batteries with organic materials as promising electrodes, Materials Today Energy, 18 (2020) 100547, https://doi.org/10.1016/j.mtener.2020.100547.

[14] Y. Zhang, Y. Liang, H. Dong, X. Wang, Y. Yao, Charge Storage Mechanism of a Quinone Polymer Electrode for Zinc-ion Batteries, Journal of The Electrochemical Society, 167 (2020) 070558, http://dx.doi.org/10.1149/1945-7111/ab847a.

[15] J. Kumankuma-Sarpong, S. Tang, W. Guo, Y. Fu, Naphthoquinone-Based Composite Cathodes for Aqueous Rechargeable Zinc-Ion Batteries, ACS Applied Materials & Interfaces, 13 (2021) 4084-4092, https://doi.org/10.1021/acsami.0c21339.

[16] B. Yang, Y. Ma, D. Bin, H. Lu, Y. Xia, Ultralong-Life Cathode for Aqueous Zinc-Organic Batteries via Pouring 9,10-Phenanthraquinone into Active Carbon, ACS Applied Materials & Interfaces, 13 (2021) 58818-58826, https://doi.org/10.1021/acsami.1c20087.

[17] Q. Zhao, W. Huang, Z. Luo, L. Liu, Y. Lu, Y. Li, L. Li, J. Hu, H. Ma, J. Chen, High-capacity aqueous zinc batteries using sustainable quinone electrodes, Science Advances, 4 (2018) eaao1761, 10.1126/sciadv.aao1761.

[18] H. Cui, P. Hu, Y. Zhang, W. Huang, A. Li, Research Progress of High-Performance Organic Material Pyrene-4,5,9,10-Tetraone in Secondary Batteries, ChemElectroChem, 8 (2021) 352-359, https://doi.org/10.1002/celc.202001396.

[19] Z. Guo, Y. Ma, X. Dong, J. Huang, Y. Wang, Y. Xia, An Environmentally Friendly and Flexible Aqueous Zinc Battery Using an Organic Cathode, angewandte chemie, 57 (2018) 11737-11741, https://doi.org/10.1002/anie.201807121.

[20] K.W. Nam, H. Kim, Y. Beldjoudi, T.-w. Kwon, D.J. Kim, J.F. Stoddart, Redox-Active Phenanthrenequinone Triangles in Aqueous Rechargeable Zinc Batteries, Journal of the American Chemical Society, 142 (2020) 2541-2548, https://doi.org/10.1021/jacs.9b12436.

[21] C. Han, J. Zhu, C. Zhi, H. Li, The rise of aqueous rechargeable batteries with organic electrode materials, Journal of Materials Chemistry A, 8 (2020) 15479-15512, http://dx.doi.org/10.1039/D0TA03947K.

[22] G. Dawut, Y. Lu, L. Miao, J. Chen, High-performance rechargeable aqueous Zn-ion batteries with a poly(benzoquinonyl sulfide) cathode, Inorganic Chemistry Frontiers, 5 (2018) 1391-1396, http://dx.doi.org/10.1039/C8QI00197A.

[23] W. Wang, V.S. Kale, Z. Cao, Y. Lei, S. Kandambeth, G. Zou, Y. Zhu, E. Abouhamad, O. Shekhah, L. Cavallo, M. Eddaoudi, H.N. Alshareef, Molecular Engineering of Covalent Organic Framework Cathodes for Enhanced Zinc-Ion Batteries, Advanced Materials, 33 (2021) 2103617, https://doi.org/10.1002/adma.202103617.

[24] K.W. Nam, S.S. Park, R. Dos Reis, V.P. Dravid, H. Kim, C.A. Mirkin, J.F. Stoddart, Conductive 2D metal-organic framework for high-performance cathodes in aqueous rechargeable zinc batteries, Nature Communications, 10 (2019) 4948, https://doi.org/10.1038/s41467-019-12857-4.

[25] Y. Gao, G. Li, F. Wang, J. Chu, P. Yu, B. Wang, H. Zhan, Z. Song, A high-performance aqueous rechargeable zinc battery based on organic cathode integrating quinone and pyrazine, Energy Storage Materials, 40 (2021) 31-40, https://doi.org/10.1016/j.ensm.2021.05.002.

[26] M. Gleria, R. De Jaeger, Phosphazenes: A worldwide insight, Nova Publishers, 2004.

[27] A.M. Amin, L. Wang, J. Wang, H. Yu, J. Huo, J. Gao, A. Xiao, Recent Research Progress in the Synthesis of Polyphosphazene and Their Applications, Designed Monomers and Polymers, 12 (2009) 357-375, https://doi.org/10.1163/138577209X12486896623373.

[28] V. Chandrasekhar, A. Chakraborty, Phosphazenes, in: Organophosphorus Chemistry: Volume 49, The Royal Society of Chemistry, 2020, pp. 349-376.

[29] S. Yeşilot, S. Küçükköylü, E. Demir, R. Demir-Cakan, Phosphazene based star-branched polymeric cathode materials via inverse vulcanization of sulfur for lithium–sulfur batteries, Polymer Chemistry, 11 (2020) 4124-4132, http://dx.doi.org/10.1039/D0PY00490A.

[30] S. Yeşilot, N. Kılıç, S. Sariyer, S. Küçükköylü, A. Kılıç, R. Demir-Cakan, A Flame-Retardant and Insoluble Inorganic–Organic Hybrid Cathode Material Based on Polyphosphazene with

Pyrene-Tetraone for Lithium Ion Batteries, ACS Applied Energy Materials, 4 (2021) 12487-12498, https://doi.org/10.1021/acsaem.1c02305.

[31] E.J. Dufek, M.L. Stone, D.K. Jamison, F.F. Stewart, K.L. Gering, L.M. Petkovic, A.D. Wilson, M.K. Harrup, H.W. Rollins, Hybrid phosphazene anodes for energy storage applications, Journal of Power Sources, 267 (2014) 347-355, https://doi.org/10.1016/j.jpowsour.2014.05.105.

[32] S.-T. Fei, H.R. Allcock, Recent Progress with Ethyleneoxy Phosphazenes as Lithium Battery Electrolytes, MRS Proceedings, 1127 (2008) 1127-T1101-1105, https://doi.org/10.1557/PROC-1127-T01-05.

[33] V. Chandrasekhar, S. Nagendran, Phosphazenes as scaffolds for the construction of multi-site coordination ligands, Chemical Society Reviews, 30 (2001) 193-203, http://dx.doi.org/10.1039/B004872K.

[34] A.R. Hillman, The EQCM: electrogravimetry with a light touch, Journal of Solid State Electrochemistry, 15 (2011) 1647-1660, https://doi.org/10.1007/s10008-011-1371-2.

[35] B. Gavriel, N. Shpigel, F. Malchik, G. Bergman, M. Turgeman, M.D. Levi, D. Aurbach, Enhanced Performance of Ti3C2Tx (MXene) Electrodes in Concentrated ZnCl2 Solutions: A Combined Electrochemical and EQCM-D Study, Energy Storage Materials, 38 (2021) 535-541, https://doi.org/10.1016/j.ensm.2021.03.027.

[36] A.D. Easley, T. Ma, C.I. Eneh, J. Yun, R.M. Thakur, J.L. Lutkenhaus, A practical guide to quartz crystal microbalance with dissipation monitoring of thin polymer films, journal of Polymer Science, 60 (2022) 1090-1107, https://doi.org/10.1002/pol.20210324.

[37] X. Zhou, S. Qiu, X. Mu, M. Zhou, W. Cai, L. Song, W. Xing, Y. Hu, Polyphosphazenes-based flame retardants: A review, Composites Part B: Engineering, 202 (2020) 108397, https://doi.org/10.1016/j.compositesb.2020.108397.

[38] M.J. Frisch, G.W. Trucks, H.B. Schlegel, G.E. Scuseria, M.A. Robb, J.R. Cheeseman, G. Scalmani, V. Barone, G.A. Petersson, H. Nakatsuji, X. Li, M. Caricato, A.V. Marenich, J. Bloino, B.G. Janesko, R. Gomperts, B. Mennucci, H.P. Hratchian, J.V. Ortiz, A.F. Izmaylov, J.L. Sonnenberg, Williams, F. Ding, F. Lipparini, F. Egidi, J. Goings, B. Peng, A. Petrone, T. Henderson, D. Ranasinghe, V.G. Zakrzewski, J. Gao, N. Rega, G. Zheng, W. Liang, M. Hada, M. Ehara, K. Toyota, R. Fukuda, J. Hasegawa, M. Ishida, T. Nakajima, Y. Honda, O. Kitao, H. Nakai, T. Vreven, K. Throssell, J.A. Montgomery Jr., J.E. Peralta, F. Ogliaro, M.J. Bearpark, J.J. Heyd, E.N. Brothers, K.N. Kudin, V.N. Staroverov, T.A. Keith, R. Kobayashi, J. Normand, K.

Raghavachari, A.P. Rendell, J.C. Burant, S.S. Iyengar, J. Tomasi, M. Cossi, J.M. Millam, M. Klene, C. Adamo, R. Cammi, J.W. Ochterski, R.L. Martin, K. Morokuma, O. Farkas, J.B. Foresman, D.J. Fox, Gaussian 16 Rev. C.01, Gaussian, Inc., Wallingford CT, (2016),

[39] H.A. Alidağı, S.O. Tümay, A. Şenocak, S. Yeşilot, Pyrene functionalized cyclotriphosphazene-based dyes: Synthesis, intramolecular excimer formation, and fluorescence receptor for the detection of nitro-aromatic compounds, Dyes and Pigments, 153 (2018) 172-181, https://doi.org/10.1016/j.dyepig.2018.02.012.

[40] Z. Tie, L. Liu, S. Deng, D. Zhao, Z. Niu, Proton Insertion Chemistry of a Zinc–Organic Battery, Angewandte Chemie International Edition, 59 (2020) 4920-4924, https://doi.org/10.1002/anie.201916529.

[41] A.B. Lamb, P.W. Carleton, W.S. Hughes, L.W. Nichols, The Copper Flame Test For Halogen In Air.1, Journal of the American Chemical Society, 42 (1920) 78-84, https://doi.org/10.1021/ja01446a011.

[42] M.J. Sanger, Flame Tests: Which Ion Causes the Color?, Journal of Chemical Education, 81 (2004) 1776A, https://doi.org/10.1021/ed081p1776A.

[43] X. Li, H.-b. Sun, X. Sun, Polysulfone grafted with anthraquinone-hydroanthraquinone redox as a flexible membrane electrode for aqueous batteries, Polymer, 234 (2021) 124245, https://doi.org/10.1016/j.polymer.2021.124245.

[44] S. Yeşilot, F. Hacıvelioğlu, S. Küçükköylü, E. Demir, K.B. Çelik, R. Demir-Cakan, A novel polyphosphazene with nitroxide radical side groups as cathode-active material in Li-ion batteries, Polymers for Advanced Technologies, 30 (2019) 2977-2982, https://doi.org/10.1002/pat.4728.

[45] N. Amarnath, D. Appavoo, B. Lochab, Eco-Friendly Halogen-Free Flame Retardant Cardanol Polyphosphazene Polybenzoxazine Networks, ACS Sustainable Chemistry & Engineering, 6 (2018) 389-402, https://doi.org/10.1021/acssuschemeng.7b02657.

[46] S. Yeşilot, S. Küçükköylü, T. Mutlu, R. Demir-Cakan, Halogen-Free Polyphosphazene-Based Flame Retardant Cathode Materials for Li–S Batteries, Energy Technology, 9 (2021) 2100563, https://doi.org/10.1002/ente.202100563.

[47] R. Emanuelsson, M. Sterby, M. Strømme, M. Sjödin, An All-Organic Proton Battery, Journal of the American Chemical Society, 139 (2017) 4828-4834, https://doi.org/10.1021/jacs.7b00159.

[48] Y. Wang, C. Wang, Z. Ni, Y. Gu, B. Wang, Z. Guo, Z. Wang, D. Bin, J. Ma, Y. Wang, Binding Zinc Ions by Carboxyl Groups from Adjacent Molecules toward Long-Life Aqueous

Zinc–Organic Batteries, Advanced Materials, 32 (2020) 2000338, https://doi.org/10.1002/adma.202000338.

[49] M. Na, Y. Oh, H.R. Byon, Effects of Zn2+ and H+ Association with Naphthalene Diimide Electrodes for Aqueous Zn-Ion Batteries, Chemistry of Materials, 32 (2020) 6990-6997, https://doi.org/10.1021/acs.chemmater.0c02357.

[50] A. Vizintin, J. Bitenc, A. Kopač Lautar, K. Pirnat, J. Grdadolnik, J. Stare, A. Randon-Vitanova, R. Dominko, Probing electrochemical reactions in organic cathode materials via in operando infrared spectroscopy, Nature Communications, 9 (2018) 661, https://doi.org/10.1038/s41467-018-03114-1.

[51] Y. Li, L. Liu, C. Liu, Y. Lu, R. Shi, F. Li, J. Chen, Rechargeable Aqueous Polymer-Air Batteries Based on Polyanthraquinone Anode, Chem, 5 (2019) 2159-2170, https://doi.org/10.1016/j.chempr.2019.06.001.

[52] L. Zeng, X. Liu, X. Chen, C. Soutis, π - π interaction between carbon fibre and epoxy resin for interface improvement in composites, Composites Part B: Engineering, 220 (2021) 108983, https://doi.org/10.1016/j.compositesb.2021.108983.

[53] H. Pan, Y. Shao, P. Yan, Y. Cheng, K.S. Han, Z. Nie, C. Wang, J. Yang, X. Li, P. Bhattacharya, K.T. Mueller, J. Liu, Reversible aqueous zinc/manganese oxide energy storage from conversion reactions, Nature Energy, 1 (2016) 16039, https://doi.org/10.1038/nenergy.2016.39.

[54] P. Lemaire, T. Dargon, D. Alves Dalla Corte, O. Sel, H. Perrot, J.-M. Tarascon, Making Advanced Electrogravimetry as an Affordable Analytical Tool for Battery Interface Characterization, Analytical Chemistry, 92 (2020) 13803-13812, https://doi.org/10.1021/acs.analchem.0c02233.

[55] G. Sauerbrey, Verwendung von Schwingquarzen zur Wägung dünner Schichten und zur Mikrowägung, Zeitschrift für Physik, 155 (1959) 206-222, https://doi.org/10.1007/BF01337937.

[56] S. Sariyer, A. Ghosh, S.N. Dambasan, E.M. Halim, M. El Rhazi, H. Perrot, O. Sel, R. Demir-Cakan, Aqueous Multivalent Charge Storage Mechanism in Aromatic Diamine-Based Organic Electrodes, ACS Applied Materials & Interfaces, 14 (2022) 8508-8520, https://doi.org/10.1021/acsami.1c19607.

[57] A.O. Efremova, A.I. Volkov, E.G. Tolstopyatova, V.V. Kondratiev, EQCM study of intercalation processes into electrodeposited MnO2 electrode in aqueous zinc-ion battery

electrolyte, Journal of Alloys and Compounds, 892 (2022) 162142, https://doi.org/10.1016/j.jallcom.2021.162142.

[58] M. Tang, S. Zhu, Z. Liu, C. Jiang, Y. Wu, H. Li, B. Wang, E. Wang, J. Ma, C. Wang, Tailoring π-Conjugated Systems: From π-π Stacking to High-Rate-Performance Organic Cathodes, Chem, 4 (2018) 2600-2614, https://doi.org/10.1016/j.chempr.2018.08.014.

[59] L. Xu, R. Shi, H. Li, C. Han, M. Wu, C.-P. Wong, F. Kang, B. Li, Pseudocapacitive anthraquinone modified with reduced graphene oxide for flexible symmetric all-solid-state supercapacitors, Carbon, 127 (2018) 459-468, https://doi.org/10.1016/j.carbon.2017.11.003.

[60] Z. Ye, S. Xie, Z. Cao, L. Wang, D. Xu, H. Zhang, J. Matz, P. Dong, H. Fang, J. Shen, M. Ye, High-rate aqueous zinc-organic battery achieved by lowering HOMO/LUMO of organic cathode, Energy Storage Materials, 37 (2021) 378-386, https://doi.org/10.1016/j.ensm.2021.02.022.

[61] D. Xu, Z. Cao, Z. Ye, H. Zhang, L. Wang, M. John, P. Dong, S. Gao, J. Shen, M. Ye, Electrochemical oxidation of π-π coupling organic cathode for enhanced zinc ion storage, Chemical Engineering Journal, 417 (2021) 129245, https://doi.org/10.1016/j.cej.2021.129245.

[62] H. Zhang, S. Xie, Z. Cao, D. Xu, L. Wang, H. Fang, J. Shen, M. Ye, Extended π-Conjugated System in Organic Cathode with Active C═N Bonds for Driving Aqueous Zinc-Ion Batteries, ACS Applied Energy Materials, 4 (2021) 655-661, https://doi.org/10.1021/acsaem.0c02526.

[63] Y. Chen, J. Li, Q. Zhu, K. Fan, Y. Cao, G. Zhang, C. Zhang, Y. Gao, J. Zou, T. Zhai, C. Wang, Two-Dimensional Organic Supramolecule via Hydrogen Bonding and π–π Stacking for Ultrahigh Capacity and Long-Life Aqueous Zinc–Organic Batteries, Angewandte Chemie International Edition, 61 (2022) e202116289, https://doi.org/10.1002/anie.202116289.

[64] G. Sun, B. Yang, X. Chen, Y. Wei, G. Yin, H. Zhang, Q. Liu, Aqueous zinc batteries using N-containing organic cathodes with Zn2+ and H+ Co-uptake, Chemical Engineering Journal, 431 (2022) 134253, https://doi.org/10.1016/j.cej.2021.134253.

[65] J. Tao, M.-L. Tong, J.-X. Shi, X.-M. Chen, S.W. Ng, Blue photoluminescent zinc coordination polymers with supertetranuclear cores, Chemical Communications, (2000) 2043-2044, http://dx.doi.org/10.1039/B005753N.